EPJ manuscript No.
(will be inserted by the editor)

Entropic, LES and Boundary Conditions in Lattice Boltzmann Simulations of Turbulence

George Vahala[1], Brian Keating[2], Min Soe[3], Jeffrey Yepez[4], Linda Vahala[5], and Sean Ziegeler[6]

[1] Department of Physics, William & Mary, Williamsburg, Virginia 23185, USA
[2] Department of Ocean and Resources Eng., University of Hawaii at Manoa, Honolulu, HI 96822, USA
[3] Department of Mathematics and Physics, Rogers State University, Claremore, OK 74017
[4] Air Force Research Laboratory, Hanscom AFB, Massachesetts 01731, USA
[5] Department of Electrical & Computer Engineering, Old Dominion University, Norfolk, Virginia 23529, USA
[6] High Performance Computing Modernization Program, Mississippi State University, MS 39762, USA

Abstract. Large scale (1600^3-grid) entropic lattice Boltzmann (ELB) simulations are performed on the 27-bit model at sufficiently high Reynolds numbers to find intermittency corrections to the Kolmogorov $k^{-5/3}$ inertial spectrum. Even though the transport coefficients in ELB and in the Large Eddy Simulation lattice Boltzmann (LES-LB) schemes have very different origins, there are strong similarities in their turbulence statistics from 512^3-grid simulations. A new lattice Boltzmann moment-space boundary condition algorithm is tested on the 2D backstep problem, with excellent agreement with experimental data even up to a Reynolds number of 800.

1 Introduction

The entropic lattice Boltzmann (ELB) scheme [1-6] permits simulation of Navier-Stokes turbulence to arbitrary Reynolds numbers. Using Q velocities on a 3D unit cube (where typically $Q = 15, 19, 27$), the ELB representation takes the form (in lattice units)

$$f_\alpha(\mathbf{x} + \mathbf{e}_\alpha, t+1) = f_\alpha(\mathbf{x}, t) - \frac{\gamma(\mathbf{x}, t)}{2\tau}\left[f_\alpha(\mathbf{x}, t) - f_\alpha^{eq}(\rho, \mathbf{u})\right], \tag{1}$$

where $\mathbf{e}_\alpha$ are the lattice vectors, τ is the bare relaxation rate giving rise to the molecular viscosity [7]

$$\nu_0 = \frac{1}{6}\left(2\tau - 1\right), \tag{2}$$

and the moments of the distribution function yield the macroscopic density and fluid velocity:

$$\sum_{\alpha=1}^{Q} f_\alpha = \rho, \quad \sum_{\alpha=1}^{Q} f_\alpha \mathbf{e}_\alpha = \rho \mathbf{u}, \tag{3}$$

In ELB [1-6] it is shown that there exists an entropy function

$$H\left[\mathbf{f}\right] = \sum_{\alpha=1}^{Q} f_\alpha \ln\left(\frac{f_\alpha}{w_\alpha}\right), \tag{4}$$

for some weights w_α, from which the collision parameter $\gamma(\mathbf{x},\mathbf{t})$ is determined by enforcing detailed balance in the local collision process: the pre- and post- collision distributions lie on the same constant entropy surface

$$H\left[\mathbf{f}\right] = H\left[\mathbf{f} - \gamma(\mathbf{f} - \mathbf{f^{eq}})\right]. \tag{5}$$

The ELB equation (1) yields an effective viscosity

$$\nu_{eff} = \frac{1}{6}\left[\frac{4\tau}{\gamma(\mathbf{x},t)} - 1\right], \tag{6}$$

In the simplest LES closure scheme [8] for the filtered Navier-Stokes equation, the Reynolds stress tensor τ_{ij} is related to the filtered mean rate of strain tensor S_{ij} by an eddy viscosity $\nu_t(\mathbf{x},t)$:

$$\tau_{ij} = \overline{u_i u_j} - \overline{u}_i\overline{u}_j = -2\nu_t S_{ij}, \tag{7}$$

where the overbar represents the filtering operation and

$$2S_{ij} = \frac{\partial\overline{u}_i}{\partial x_j} + \frac{\partial\overline{u}_j}{\partial x_i}, \quad \text{with} \quad \nu_t = (C_s\triangle)^2\sqrt{S_{ij}S_{ij}}. \tag{8}$$

In LES-LB [9,10], it can be shown that the mean rate of strain tensor at the macroscopic level is determined by the local moments of the non-equilibrium (filtered) distribution function at the mesoscopic level

$$S_{ij} = -\frac{3}{2\rho\tau}\sum_{\alpha=1}^{Q} e_{\alpha i}e_{\alpha j}\left(f_\alpha - f_\alpha^{eq}\right), \tag{9}$$

where τ is the simple Bhatnagar-Gross-Krook relaxation rate determining the molecular viscosity, Eq. (2).

It should be noted that the ideal parallelization of the lattice Boltzmann algorithm is not compromised by either the ELB nor LES-LB since all the extra computations are purely local.

2 High Reynolds number ELB simulations on the $Q27$ lattice

The $Q27$ model entails streaming velocities of speed (and number of velocities) is the following: 0 (1), 1 (6), $\sqrt{2}$ (12), $\sqrt{3}$ (8). We consider the evolution of energy spectra from an initial Kida [11] velocity:

$$\mathrm{u_x}\left(\mathbf{x}, t=0\right) = U_\circ\left[\cos 3y\cos z,\ -\cos y\cos 3z,\ \sin x\right], \tag{10}$$

with cyclic permutations for u_x and u_y. The simulations are performed on a 1600^3-grid at an initial Reynolds number of 25000. The evolution of the 1D transverse energy spectrum

$$E_t(k_x,t) = \sum_{k_y k_z}|u_y(k_x,k_y,k_z,t)|^2, \quad \text{with} \quad \mathrm{E_t(k_x, t=0)} \approx \delta(\mathrm{k_x}-2) + \delta(\mathrm{k_x}-4). \tag{11}$$

is shown in Fig. 1 for times t = 28K to 54K. The Kolmogorov $k^{-5/3}$ spectrum spectrum is shown as a dashed line in Fig. 1a. Moreover, one can infer the slight deviation $k^{-0.1}$ from the Kolmogorov $k^{-5/3}$ spectrum (Fig. 1b for times $t = 28K$ and $38K$). This deviation, first seen in the pseudo-spectral simulations of Kaneda [12] on a 4800^3-grid, is attributable to intermittency.

The corresponding probability distribution functions, shown in Fig. 2, for the x-component of velocity $P(u_x)$ and vorticity $P(\omega_x)$ bear this out : $P(u_x)$ is quasi-Gaussian while $P(\omega_x)$ is quasi-exponential. The Gaussian and exponential pdfs are shown dashed in Fig. 2.

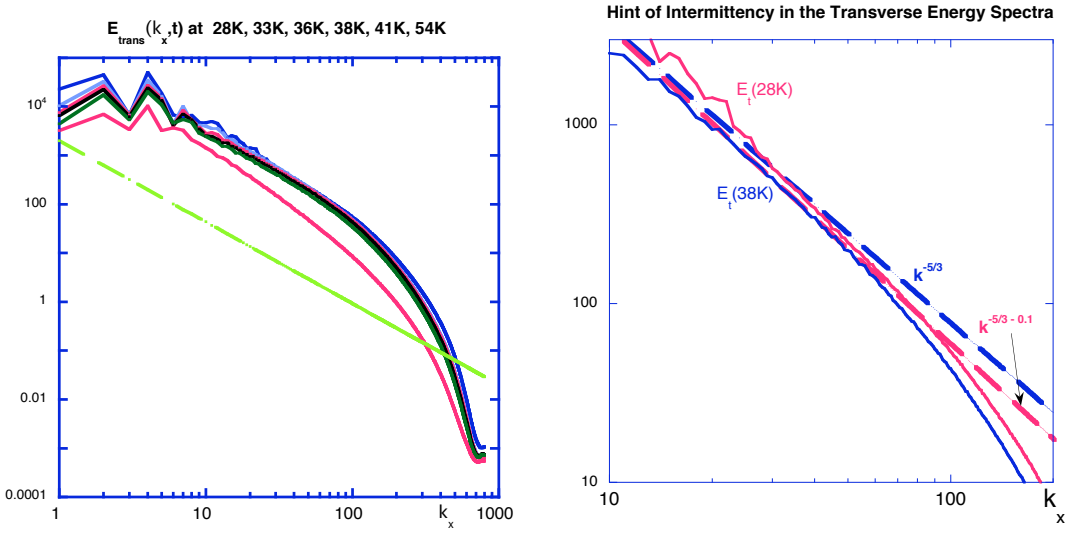

Fig. 1. The 1D energy spectrum for various times, in lattice units (left). The dashed green line is the Kolmogorov $k^{-5/3}$ spectrum. A blow-up in k_x-space of the 1D energy spectrum (right). The dashed lines are the $k^{-5/3}$ (Kolmogorov) and $k^{-5/3-0.1}$ (intermittent) spectra.

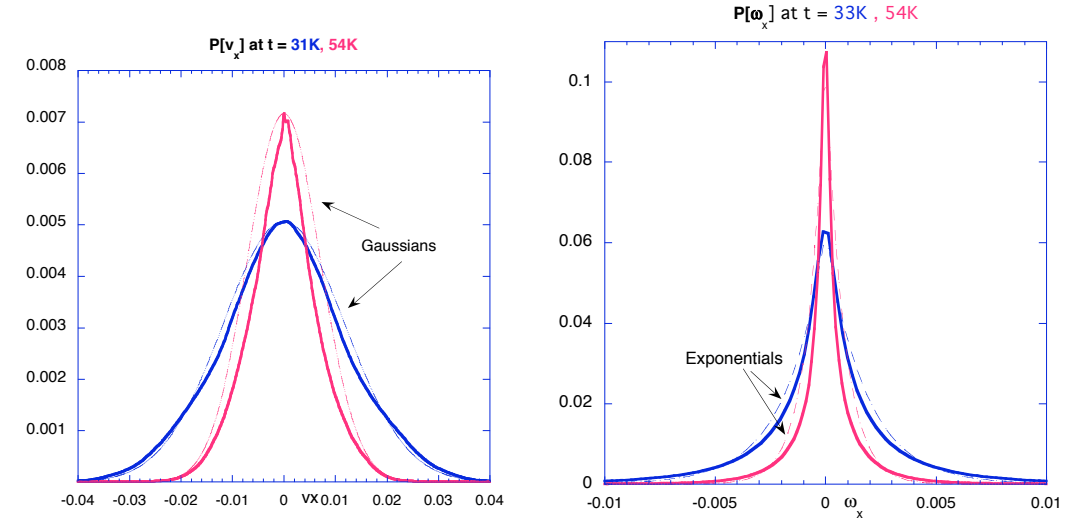

Fig. 2. The probability distribution functions for the x-component of velocity (left) and vorticity (right) and contrasted with theoretical Gaussian and exponential pdfs (dashed).

3 A comparison between lattice Boltzmann, LES-LB and ELB models

For the $Q27$-model, we show the time decay of the energy moments for the various lattice Boltzmann models for bare viscosities, Eq. (2), $\nu_0 = 2 \times 10^{-3}$ and $\nu_0 = 2 \times 10^{-4}$. At this lower viscosity, the simple lattice Boltzmann model is numerically unstable. In the LES-LB algorithm we choose a filter width $\triangle = 1$ (in LB units) and vary the Smagorinsky constant in the LES-LB model. The simulations were performed on a 512^3-spatial grid.

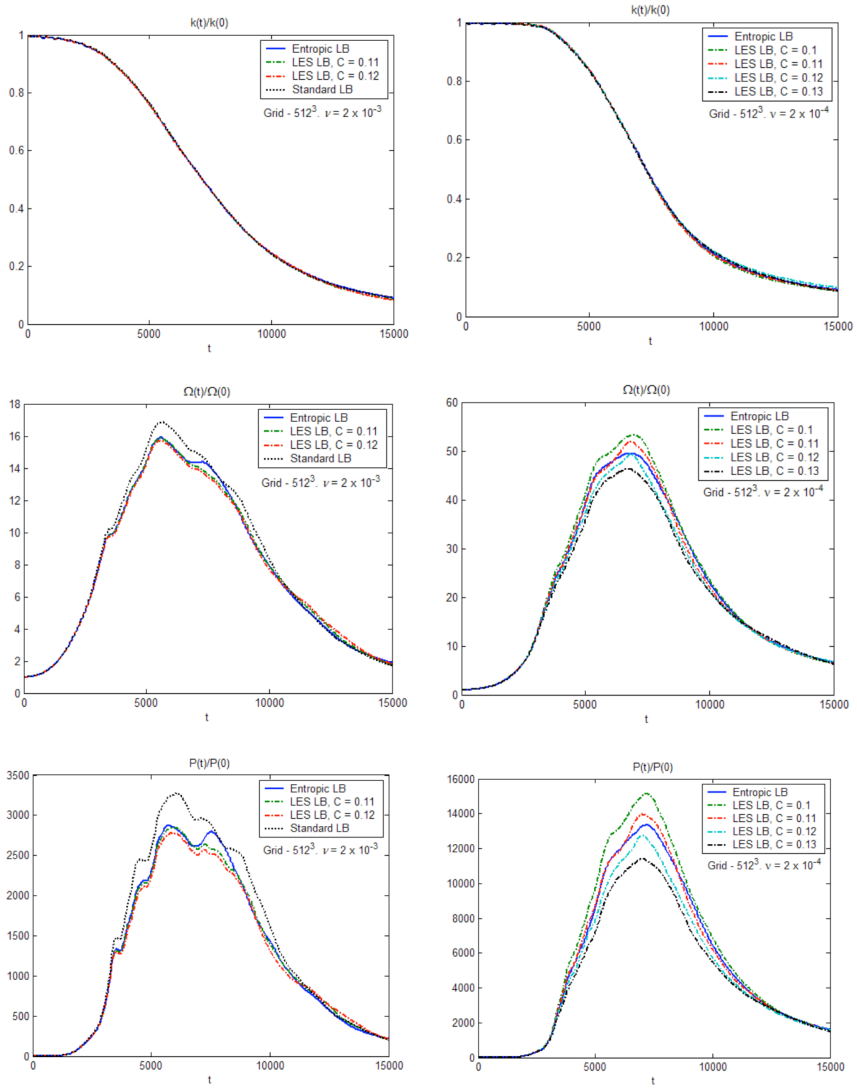

Fig. 3. The decay of the kinetic energy k(t), enstrophy $\Omega(t)$ and palinstrophy $P(t)$ for two different bare viscosities using the $Q27$ model. The plots in the left column are for the low bare viscosity run $\nu_0 = 2\times10^{-3}$, while the plots in the right column are for $\nu_0 = 2\times10^{-4}$. Very good agreement is obtained between ELB and LES-LB for $C_s = 0.11$. As expected, ELB is more dissipative than standard lattice Boltzmann.

The rapid initial rise of the enstrophy (till about $t = 4000$) is due to inviscid vortex stretching. This inviscid stretching time interval can also be seen in the strong flattening of the initial kinetic energy for $t = 4000$ in Fig. 3. The peaking in the enstrophy is inversely proportional to the total viscosity. As expected and seen in Fig. 3, ELB is more dissipative than LB. For higher Reynolds numbers, lattice Boltzmann is numerically unstable. In Fig. 3b we continue to see excellent agreement between ELB and LES-LB for Smagorinsky constant $C_s = 0.11$. Of course, it should be pointed out that ELB is parameter-free while LES-LB is strongly dependent on the Smagorinsky constant, a free parameter in the LES model.

4 Boundary Conditions in 2D LB-Navier Stokes: Reattachment in the flow over a backstep

Incompressible flow over a backstep is considered up to Reynolds number Re = 800. We restrict our simulations to 2D, using the simple lattice Boltzmann 9-bit model since the Reynolds number is sufficiently low for the model to be numerically stable. The inlet mean velocity profile is chosen to be the standard parabolic profile for fully developed laminar channel flow, with $H_2 = 2H_1$ and $H = H_1$, while the outflow is handled by first order extrapolation. No-slip boundary conditions are applied at the walls.

In the lattice Boltzmann model further boundary conditions must be specified. Here we introduce the idea of moment-space boundary conditions. To apply boundary conditions, we do not work in the usual $\{f_\alpha, \alpha = 1 \dots 9\}$-space but rather in the 9-moment set

$$\mathbf{M} = \{\rho, \rho\mathbf{u_x}, \rho\mathbf{u_y}, \mathbf{\Pi_{xy}}, \mathbf{\Pi_{yy}}, \mathbf{\Pi_{xy}}, \mathbf{N}, \mathbf{J_x}, \mathbf{J_y}\}^{\mathbf{T}} = \{\mathbf{M_1}, \mathbf{M_2}, \cdots, \mathbf{M_9}\}^{\mathbf{T}}, \tag{12}$$

where the first 6 moments are the standard fluid moments. The pressure tensor $\Pi_{ij} = \rho\,\delta_{ij}/3 + \rho u_i u_j$. The remaining 3 independent non-hydrodynamic moments are somewhat arbitrary and here are chosen as follows [13]:

$$N = \sum_{\alpha=1}^{9} f_\alpha g_\alpha, \quad \mathbf{J} = \sum_{\alpha=\mathbf{1}}^{\mathbf{9}} \mathbf{f}_\alpha \mathbf{e}_\alpha \mathbf{g}_\alpha, \quad \text{where} \quad \mathbf{g} = \{\mathbf{1}, -\mathbf{2}, -\mathbf{2}, -\mathbf{2}, -\mathbf{2}, \mathbf{4}, \mathbf{4}, \mathbf{4}, \mathbf{4}\}^{\mathbf{T}}. \tag{13}$$

There is a 1-to-1 transformation between $\{\mathbf{f}\}$ and $\{\mathbf{M}\}$. The evolution equations for the non-hydrodynamic moments are readily derived using the standard Chapman-Enskog expansions. With the usual $\mathbf{f^{eq}}$, the evolution of $N, \mathbf{J}$ will now not influence the mean velocity (although their evolution, of course, is affected by $\mathbf{u}$). This decoupling is viewed as a strength of our new method. The aim is to minimize artificial gradients near the boundaries. On the walls, $M_1 = \rho$ is determined from the known distribution function set using the method outlined in Zou-He [14]. The no-slip boundary conditions determine the moments M_2, M_3 and the equilibrium part of the stresses $M_4, \cdots, M_6$. The only unknowns are the non-hydrodynamic moments M_7, M_8, M_9 at the walls. While we considered various schemes to determine these moments and the non-equilibrium parts of the stresses at the walls, the simplest scheme that worked well for our backstep problem was just a shift of these moments values from the spatial nodes nearest the wall node to the wall node. This scheme yielded stable computations for the 2D backstep flow problem to Re = 1066. Our simple application of the Zou-He boundary conditions only permitted us to attain Re = 80.

As seen in Fig. 4, our moment boundary condition scheme yields excellent results for the reattachment length as a function of Reynolds number all the way to Re = 800 as compared to the experimental data of Armaly et. al. [15]. The 2D CFD simulations results yield quite low reattachment lengths at Re = 600 and Re = 700. The Karlin groups LB data [16] is given only up to Re = 400 and it seems to be asymptoting away from the experimental results. The Succi groups data [17] is only presented to Re = 200. The 3D CFD simulations [18], as might be expected, give very good results. While this is the first application of moment-methods to boundary condition, it has been introduced here to handle the collision step in the lattice Boltzmann algorithm [13] because of local collisional invariants.

5 Acknowledgements

This work was supported by AFOSR and DoE with much computational resources of NERSC, and DoD MSRC sites at NAVO and AFRL.

References

1. I. V. Karlin, A. Ferrante, H. C. Ottinger, *Europhys. Lett*, **4**,182 (1999).

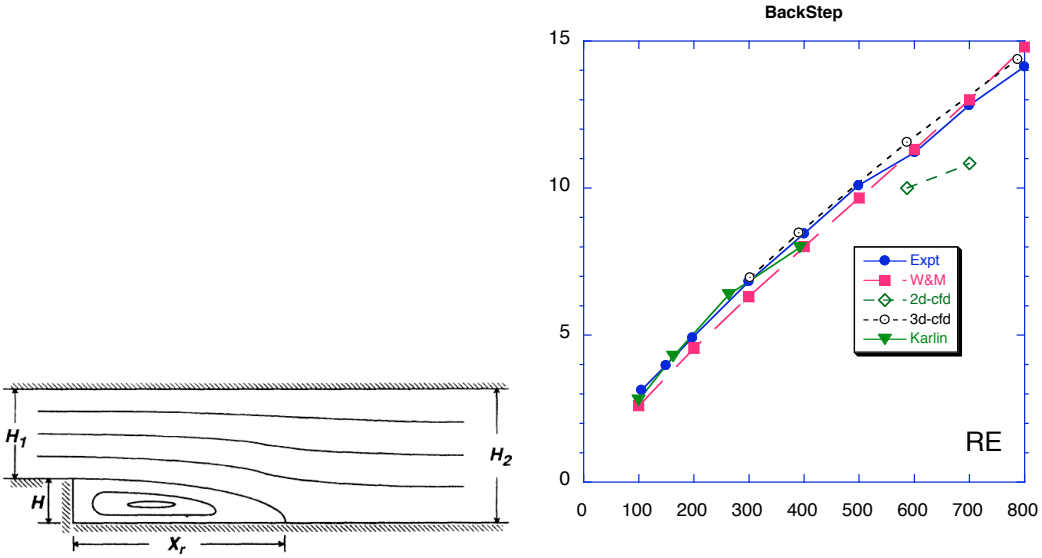

Fig. 4. Flow over a backstep. The reattachment length X_r/H is plotted as a function of Re. Our moment space boundary condition method accurately predicts the reattachment length to Re = 800 [red squares]. The experimental data is presented in blue dots. Other lattice Boltzmann and CFD results are also plotted.

2. S. Ansumali, I. V. Karlin, *Phys. Rev.*, **E62**,7999 (2000); **E65**, 056312 (2000)
3. S. Ansumali, I. V. Karlin, *Phys. Rev. Lett.*, **95**, 260604 (2005).
4. B. M. Boghosian, J. Yepez, P. V. Coveney, A. Wagner *Proc. R. Soc. Lon. Ser A*, **457**, 717 (2001)
5. B. M. Boghosian, P. J. Love, J. Yepez, P. V. Coveney, *Physica D* **193**, 169 (2004)
6. B. Keating, G. Vahala, J. Yepez, M. Soe, L. Vahala, *Phys. Rev. E* **75**, 036712 (2007).
7. S. Succi. *Lattice Botlzmann Equation for Fluid Dynamics and Beyond*, (Oxford, 2001)
8. J. Smagorinsky. *Mon. Weather Rev.*, **91**, 99 (1963).
9. S. Hou, J. Sterling, S. Chen, G. D. Doolen, in *Pattern Formation and Lattice Gas Automata*, ed. A. T. Lawniczak, R. Karpal in *Field Inst. Commun.* **6**, 151 (1996).
10. H. Yu, S. S. Girimaji, L-S. Luo, *J. Computat. Phys.* **209**, 599 (2005)
11. S. Kida, Y. Murakami, *Phys. Fluids* **30**, 2030 (1987)
12. Y. Kaneda, T. Ishihara, M. Yokokawa, K. itakura, A. Uno, *Phys. Fluids* **15**, L21 (2005)
13. P. Lallemand, L-S. Luo, *Phys. Rev. E* **61**, 6546 (2000)
14. Q. Zou, X. He, *Phys. Fluids* **9**, 1591 (1997)
15. B. F. Armaly, F. Durst, J. C. F. Pereira, B. Schonung, *J. Fluid Mech.* **127**, 473 (1983)
16. S. S. Chikatamarla, S. Ansumali, I. V. Karlinr, *Europhys. Lett*, **7**, 215 (2006).
17. S. Ubertini, S. Succi, *Comput. Fluid Dyn.*, **5**, 85 (2005)
18. L. K. Kaiktsis, G. E. Karniadakis, S. A. Orszag, *J. FLuid Mech.*, **231**, 501 (1991)